JOURNAL OF GUIDANCE, CONTROL, AND DYNAMICS
Vol. 34, No. 1, January–February 2011

Robust Roll Autopilot Design for Tactical Missiles

S. E. Talole,* A. A. Godbole,† and J. P. Kolhe*
Defence Institute of Advanced Technology, Girinagar, Pune 411 025, India
and
S. B. Phadke‡
College of Engineering Pune, Shivajinagar, Pune 411 005, India

DOI: 10.2514/1.50555

In this paper, a robust roll autopilot based on the extended state observer technique is proposed. The autopilot is robust to uncertainties, external disturbances, the airframe flexibility, and fast unmodeled sensor lags. The external disturbances and the parametric uncertainties in the roll loop are treated as a composite disturbance and the extended state observer is used to estimate the composite disturbance and the states of the system in an integrated manner. The estimated disturbance and the estimated states are used to robustify linear quadratic regulator autopilots designed for nominal systems. The closed-loop stability of the observer-controller combination is proved. Simulation results are presented to demonstrate the efficacy of the extended state observer in estimation of the uncertainties and the states, and in meeting the objectives of the design. Lastly, the proposed design is compared with some well-known designs reported in the literature.

I. Introduction

UNLIKE aircraft, there is no strongly stable position in roll for cruciform, Cartesian controlled missiles, and therefore they tend to roll due to various undesirable rolling moments such as the ones arising from airframe misalignments, asymmetrical loading of the lifting and control surfaces, fin biases, and atmospheric disturbances. In most missiles, the roll position is required to be stabilized because the rolling motion leads to several undesirable effects [1,2]. For missiles that are stabilized in roll position, the pitch and yaw channels can be considered as decoupled single-input single-output systems, thereby greatly simplifying the design of the lateral autopilots.

Because of the uncertainties in aerodynamic parameters, airframe flexibility, unmodeled dynamics, cross coupling, external disturbances, nonlinearities, and measurement inaccuracies, the problem of designing roll autopilots that can guarantee stability and performance throughout the flight envelope is a challenging one. Conventionally, missile autopilots are designed by gain scheduling for missile models linearized around several operating points in the flight envelope, which explains the dominance of classical linear control techniques in missile autopilot designs for several decades in the past [1,3,4]. On the other hand, one also finds some applications of various modern and advanced control theories in the design of autopilots for tactical missiles. Design of roll autopilots based on the H_∞ approach [5], μ analysis [6,7], optimal control [8–12], variable structure control [13], dynamic inversion [14], and dynamic inversion combined with a neural network [15] are some examples worth citing. While the modern control techniques offer powerful tools for autopilot design, they suffer from certain shortcomings when put to practice. Many modern control approaches require an exact mathematical model of the system in terms of its structure and parameters. In practice, it is hard to get an exact model of the system, resulting in designs that do not offer the intended performance. Direct application of modern techniques to realistic models of missile dynamics, leads to complex control strategies that require additional instrumentation/sensors. On the other hand, controllers designed using simplified/reduced order models may lead to instability when the unmodeled dynamics gets excited [8,9]. It is shown in [9] that an optimal roll controller designed using a simplified model results in an unstable system when applied to a more realistic model of the system. In [8,9], the issue of unmodeled dynamics is addressed by combining the design of a modern controller with the concepts in the classical control theory. The authors have shown that by adjusting the weightings in the performance measure, it is possible to retain the optimal performance in the presence of fast unmodeled dynamics. However the resulting design does not offer satisfactory performance when the system is subjected to an external disturbance. Another issue to deal with in the implementation of modern controllers, is the requirement of the availability of the complete state vector.

While the requirement of the state vector can be met by designing an appropriate observer, the issue of external disturbances and uncertainties needs attention. One strategy to address this issue, is to treat the effects of disturbances and uncertainties as a composite disturbance acting on the system, to estimate it and then to use the estimate in the control to cancel the effect of the disturbance. As the real world plants are usually affected by significant uncertainties and unmeasurable external disturbances, disturbance rejection or compensation has become an important problem in the design high performance control systems. A great deal of effort has been devoted to address this issue and consequently a number of methods/approaches are proposed to robustify systems in the presence of the uncertainties and disturbances. For example, in [16], the theory of time delay control (TDC) is presented, wherein a function representing the effect of uncertainties and external disturbances is estimated directly using the information in the recent past and then a control is designed using this estimate in such a way as to cancel out the effect of the uncertainties and the external disturbances. An application of the TDC to estimate the target acceleration in a missile guidance scheme can be found in [17]. In [18], an input–output linearizing controller is robustified by estimating the uncertainties using the recently developed uncertainty and disturbance estimation approach. The estimation of uncertainties can also be used to overcome some well-known drawbacks in the sliding mode control as shown in [19]. In [20], a sliding mode disturbance observer is designed to estimate the uncertainties and disturbances acting on the system and then the estimate is used to compensate the effect of the uncertainties. Applications of disturbance estimation and rejection can also be found in autopilot design problems. For example, in [11] an observer is designed for the roll channel to estimate the

Received 29 April 2010; revision received 9 September 2010; accepted for publication 9 September 2010.

*Scientist, Department of Aerospace Engineering.
†Doctoral Student, Department of Aerospace Engineering.
‡Professor Emeritus, Department of Instrumentation and Control.

aerodynamic disturbance term. Similarly, in [15] a neural network based adaptive element is added to the dynamic inversion based controller for the purpose of compensation of inversion errors.

The roll autopilots can be made robust by employing any of the strategies for disturbance estimation and compensation stated above, in conjunction with the modern controllers designed for nominal systems. However, as stated earlier, the implementation of modern controllers needs the complete state vector which is not available in general. Therefore, it is necessary to be able to estimate the uncertainties and disturbances along with the complete state vector. This requirement is met by the extended state observer (ESO) [21–24], which estimates the uncertainties and disturbances and the states in an integrated manner.

In this paper, the problem of designing a roll autopilot that is implementable and is robust to uncertainties and external disturbances as well as fast unmodeled dynamics is addressed. Our approach involves the following steps: 1) design a roll autopilot for the nominal system using the linear quadratic regulator (LQR) technique, 2) using the ESO, estimate the effects of the external disturbances and uncertainties as well as the states of the system in an integrated manner, and 3) use the estimate of the uncertainties and disturbances to robustify the LQR controller and use the estimate of the states to make it implementable. In [9], the gain crossover frequency is reduced by adjusting the weightings in the LQR performance measure so as to avoid the stability problems arising from the unmodeled dynamics. However, the resulting design remains sensitive to external disturbances. In this work, no adjustment of the weighting factors in the LQR is needed as the effects of the unmodeled dynamics are mitigated by the use of the estimated states for feedback [25,26]. The design does not require any knowledge of the characteristics (such as bounds) of the uncertainties/disturbances acting on the system. The closed-loop stability of the system under the proposed controller-observer structure is proved. Simulations are carried out in the presence of external disturbances, parametric uncertainties, airframe flexibility, sensor dynamics, and measurement noise, and the results demonstrate the efficacy of the proposed approach. Lastly, the proposed design is compared with the designs presented in [8,9]. The paper is organized as follows: Sec. II presents the roll autopilot problem and the design of an LQR controller for roll position stabilization. In Sec. III, the theory of ESO is briefly reviewed and applied to the present problem. The stability of the system under the proposed design is discussed in Sec. IV. Simulation results demonstrating the effectiveness of the proposed design in a realistic scenario are given in Sec. V. The results of a comparative study of the proposed design with some of the existing designs are presented in Sec. VI, and finally Sec. VII concludes this work.

II. Roll Autopilot Problem

A great majority of missiles have a symmetrical cruciform configuration so that they can maneuver quickly and accurately in any direction. Because of the lack of inherent stability in roll, such missiles tend to roll in response to roll disturbance moments acting on them. To overcome the undesired effects of rolling motion, most missiles are equipped with autopilots to stabilize the roll position in spite of the disturbance moments. The design goal for such autopilots is to maintain the stability and the performance over the entire flight envelope.

A realistic block diagram of the roll autopilot is shown in Fig. 1e, in which a rate gyro is used as a sensor and the roll angle is obtained by integrating its output. The actuator is modeled by a second-order transfer function. Traditionally, autopilots are designed by considering only the rigid body dynamics of the missile with sufficient stability margins being provided to cater for the ignored/unmodeled dynamics such as the flexibility effects and sensor dynamics. However, since missiles are flexible bodies, the rate gyro senses the torsional modes as well. To account for this reality, a transfer function representing the dynamics of the first torsional mode is included in the autopilot block diagram. The dynamics of the rate gyro is also included. Lastly in reality, missiles are subjected to disturbance moments in the roll loop which are treated as external disturbances. To this end, it is assumed that the missile is acted upon by a disturbance moment L_d, resulting in a roll acceleration of d_{ext} [1,7].

A. Mathematical Model

Under the assumption of decoupled roll, pitch, and yaw channels, the transfer function that forms the basis of roll autopilot design is [1,9] shown in Fig. 1 and is reproduced here for the sake of completeness

$$\frac{\phi(s)}{\delta(s)} = \frac{K_\delta}{s(s+\omega_{\text{RR}})} \tag{1}$$

where ϕ is the roll angle, δ is the aileron deflection, K_δ is the fin effectiveness, and ω_{RR} is the roll rate bandwidth. The servo dynamics is given by

$$\frac{\delta(s)}{\delta_c(s)} = \frac{\omega_A^2}{(s^2 + 2\zeta_A\omega_A s + \omega_A^2)} \tag{2}$$

where ω_A, ζ_A are resp. the natural frequency and the damping ratio of the actuator and δ_c is the commanded aileron deflection. In view of Eqs. (1) and (2), the transfer function from $\delta_c(s)$ to $\phi(s)$ can be written as

$$\begin{aligned}\frac{\phi(s)}{\delta_c(s)} &= \frac{\omega_A^2}{s(s^2 + 2\zeta_A\omega_A + \omega_A^2)}\frac{K_\delta}{(s+\omega_{\text{RR}})} \\ &= \frac{b}{s^4 + a_1 s^3 + a_2 s^2 + a_3 s + a_4}\end{aligned} \tag{3}$$

where $b \triangleq K_\delta\omega_A^2$, $a_1 \triangleq 2\zeta_A\omega_A + \omega_{\text{RR}}$, $a_2 \triangleq 2\zeta_A\omega_A\omega_{\text{RR}} + \omega_A^2$, $a_3 \triangleq \omega_{\text{RR}}\omega_A^2$, and $a_4 \triangleq 0$. In the presence of uncertainties in the aerodynamic derivatives, the terms a_i $i = 1$–4 and b will not be known precisely. This is accounted for by modeling the parameters as $a_i = a_{io} + \Delta a_{io}$ and $b = b_o + \Delta b$ where a_{io} and b_o denote the nominal values of the respective parameters, while Δa_i, Δb are the corresponding uncertainties. Considering these uncertainties, the dynamics given by Eq. (3) can be rewritten in the phase variable state-space model as

$$\dot{x}_p = A_p x_p + B_p u + B_d d \qquad y_p = C_p x_p \tag{4}$$

where $x_p = [x_1 \quad x_2 \quad x_3 \quad x_4]^T$ is the state vector, $y_p = \phi$ is the output, $u = \delta_c$ is the commanded aileron deflection, B_d is the disturbance input matrix, and A_p, B_p, and C_p are the system matrices given by

$$A_p = \begin{bmatrix} 0 & 1 & 0 & 0 \\ 0 & 0 & 1 & 0 \\ 0 & 0 & 0 & 1 \\ -a_{4o} & -a_{3o} & -a_{2o} & -a_{1o} \end{bmatrix}, \qquad B_p = \begin{bmatrix} 0 \\ 0 \\ 0 \\ b_o \end{bmatrix}$$

$$B_d = \begin{bmatrix} 0 \\ 0 \\ 0 \\ 1 \end{bmatrix}, \quad \text{and} \quad C_p = [1 \quad 0 \quad 0 \quad 0]$$

The variable d is the composite disturbance representing the net effect of the parametric uncertainties and the external disturbance acting on the system and is defined as

$$d \triangleq -\Delta a_4 x_1 - \Delta a_3 x_2 - \Delta a_2 x_3 - \Delta a_1 x_4 + \Delta b u + w \tag{5}$$

where w represents the external disturbance.

B. LQR Controller

The objective of the design is to control the roll attitude of the missile with a satisfactory transient while keeping the roll angle, the roll rate and the aileron deflection within specified limits. While it is possible to design the controller by a variety of methods, an LQR controller [8] is preferred here. The LQR is designed to minimize a

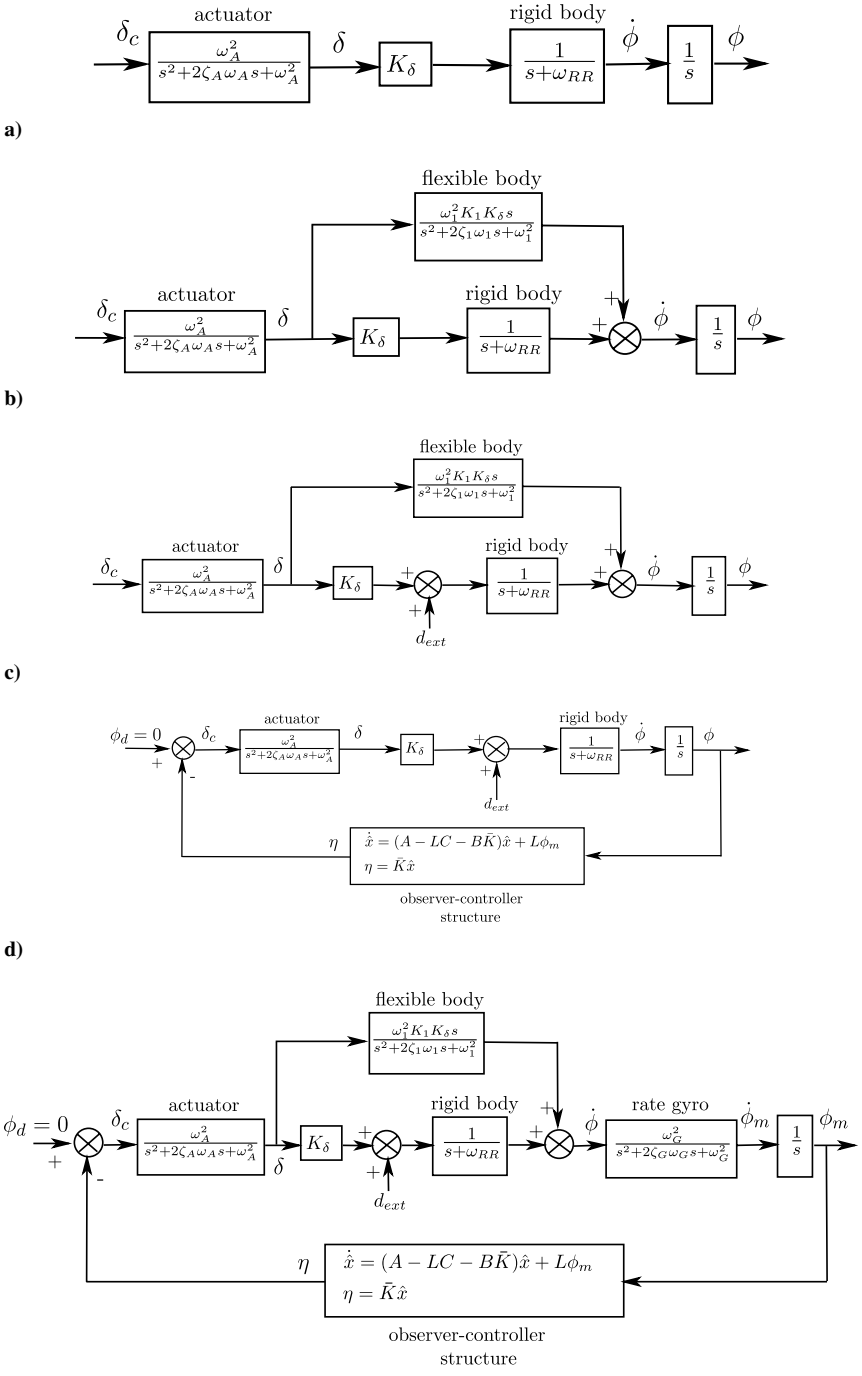

Fig. 1 System block diagrams.

quadratic performance measure of the form $J = \int_0^\infty (x_p^T Q x_p + u^T R u)\, dt$ where $Q \geq 0$ and $R > 0$, are the weightings to be chosen by the designer. The resulting optimal control law, which henceforth will be referred to as the LQR controller, is given by

$$u = -Kx_p \tag{6}$$

where $K = R^{-1}B_p^T P$ where P is the solution to the algebraic Matrix Riccatti equation, $PA_p + A_p^T P - PB_p R^{-1} B_p^T P + Q = 0$. The weightings Q and R are chosen as [8]

$$Q = \begin{bmatrix} \frac{1}{\phi_{\max}^2} & 0 & 0 & 0 \\ 0 & \frac{1}{\dot{\phi}_{\max}^2} & 0 & 0 \\ 0 & 0 & 0 & 0 \\ 0 & 0 & 0 & 0 \end{bmatrix}; \qquad R = \begin{bmatrix} \frac{1}{\delta_{c(\max)}^2} \end{bmatrix} \tag{7}$$

where $\phi_{\max}$, $\dot{\phi}_{\max}$, and $\delta_{c(\max)}$ are the maximum permissible values of the respective variables. Obviously by choosing the values of the weightings Q and R appropriately, one can obtain the desired performance.

C. Performance of the LQR Controller

The performance of the LQR controller of Eq. (6) is assessed thorough simulation using the data taken from [8] and shown in Table 1. The LQR controller gain K is obtained by taking the weightings Q and R given in Eq. (7) with the values for $\phi_{\max}$, $\dot{\phi}_{\max}$, and $\delta_{c(\max)}$ taken from Table 1. The initial roll angle is assumed to be 10° while the other initial conditions for the plant are taken as 0, giving $x_p(0) = [\,10^\circ \quad 0 \quad 0 \quad 0\,]^T$. Because the LQR needs the states, the same were obtained by numerical differentiation of the output. Simulations are carried out using the LQR controller of

Table 1 Simulation parameters

ω_{RR}	Roll rate bandwidth	2 rad/s
K_δ	Fin effectiveness	9000 $1/s^2$
ω_A	Actuator bandwidth	100 rad/s
ζ_A	Actuator damping	0.65
ω_G	Rate gyro bandwidth	200 rad/s
ζ_G	Rate gyro damping	0.5
ω_1	Torsional mode frequency	250 rad/s
ζ_1	Torsional mode damping	0.01
K_1	Torsional mode gain	−0.0000129
ϕ_{max}	Maximum desired roll angle	10 deg
$\dot{\phi}_{max}$	Maximum desired roll rate	300 deg/s
$\delta_{c(max)}$	Maximum desired fin deflection	30 deg
d_{ext}	External disturbance	200 rad/s^2
ω_N	Notch filter numerator frequency	250 rad/s
ζ_N	Notch filter numerator damping	0.01
ω_D	Notch filter denominator frequency	250 rad/s
ζ_D	Notch filter denominator damping	0.5

Eq. (6) as applied to the system of Fig. 1a and the results are presented in Fig. 2. From the figures, it can be noted that the controller has regulated the roll angle to zero as desired and also the commanded aileron deflection is within the desired limits of $\pm 30°$. Note that the settling time for the roll angle appears to be large in comparison to the settling time that can be obtained in the current tactical missile roll autopilots. The simulation results correspond to the data of the missile and the servo given in Table 1. It may be noted that current missiles employ servos of much higher bandwidth and also have a higher fin effectiveness than the ones given in Table 1 and so the use of such data will result in a smaller time constant. As the purpose of this work is to demonstrate the efficacy of the proposed ESO-based controller, the data of Table 1 is used for the rest of the simulations as well. Next, to assess the performance of the LQR controller of Eq. (6) in the presence of unmodeled dynamics, simulations are carried out by considering the effect of flexibility. To this end, the first torsional mode shown in Fig. 1b is included in the simulation and the corresponding results are presented in Fig. 3. From the figures, it can be observed that the inclusion of flexibility dynamics has rendered the LQR controller unstable. In [9], it has been shown that the stability of the LQR controller can be recovered by adjusting the weightings to lower the open-loop gain crossover frequency so that the unmodeled dynamics is not excited. Also, it is shown in [9] that the change in the weighting R has a more profound effect on the frequency response. However, the resulting design would not offer satisfactory performance, i.e., zero roll angle error in the presence of an external disturbance.

As seen from Fig. 3, the LQR controller goes unstable in the presence of the flexibility effect. It is important to note that the controller employed the true states (i.e., the one obtained through numerical differentiation of ϕ) for feedback purpose. In [25,26], it has been shown that the performance of such state feedback controllers in the presence of unmodeled dynamics is better if the estimated states are used instead of the actual states. To show this, a Luenberger observer (LO) [27] is designed for the dynamics given by Eq. (4). The observer gains are obtained by placing the poles of the

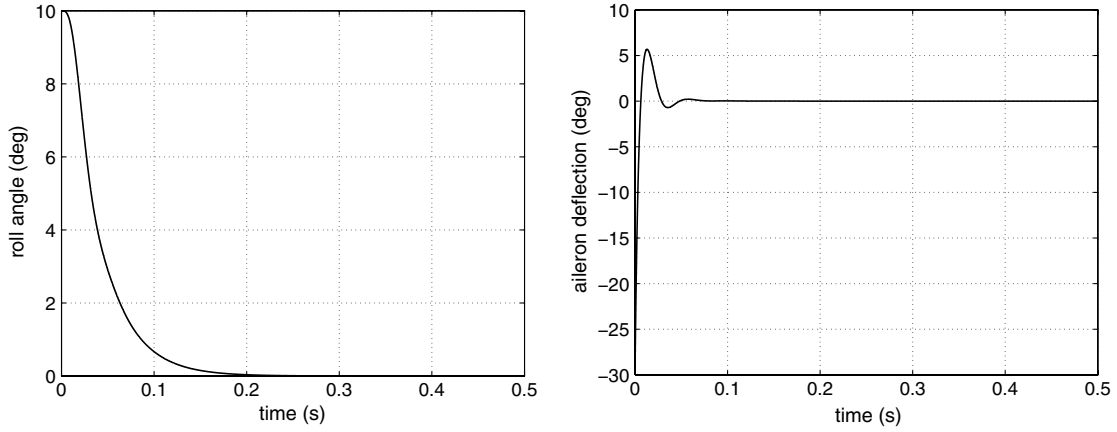

a) b)

Fig. 2 Performance of LQR controller.

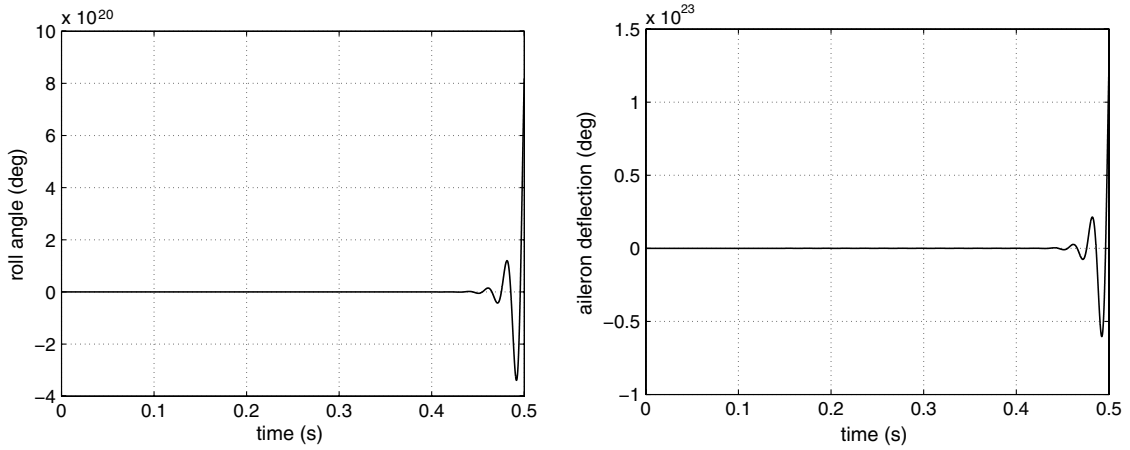

a) b)

Fig. 3 Performance of LQR controller with flexibility dynamics.

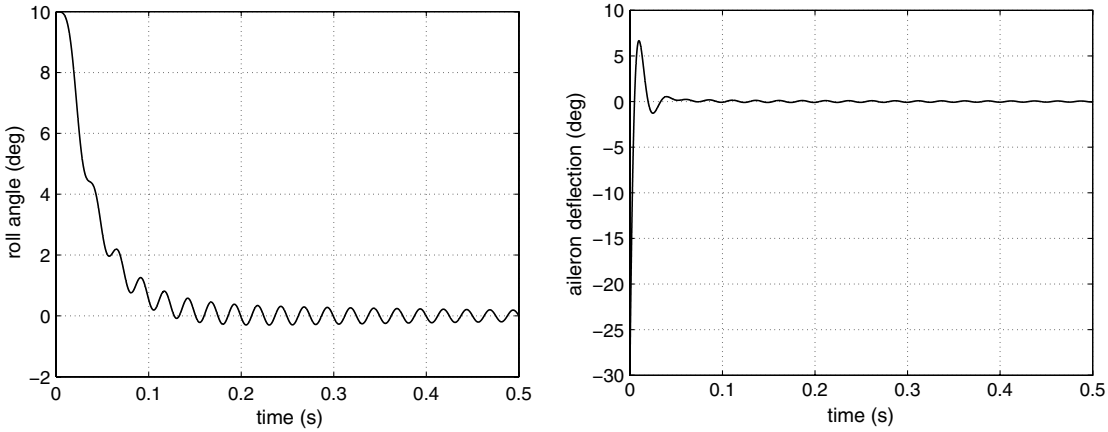

a) b)

Fig. 4 Performance of LQR + LO controller with flexibility dynamics.

observer error dynamics at −45. Simulations are carried out with the LQR controller implemented using the estimated states in the presence of flexibility dynamics and the results are as shown in Fig. 4. Comparing Figs. 3 and 4, it can be noticed that while the system goes unstable when true states are used in the LQR controller, the same controller offers a stable performance when implemented using the estimated states. Next, we include the external disturbance along with the flexibility dynamics as shown in Fig. 1c and the simulation results of the LQR controller using the estimated states are presented in Fig. 5. Once again it is seen that although the LQR controller offers stability, the performance is degraded as there exists a steady-state error in the roll attitude. Thus, although the issue of unmodeled dynamics can be handled either by adjusting the weighting or by the use of estimated states, from external disturbance point of view, neither of them gives the desired performance in regulation of the roll position and thus the issue needs attention.

The problem of roll autopilot design, considered in this paper, can be characterized as a problem of controlling the system in the presence of both the structured uncertainties and the unstructured uncertainties. The structured uncertainties can be estimated and compensated for by a variety of methods as pointed out previously in the paper. The unstructured uncertainties are caused by unmodeled lags and are somewhat harder to deal with because they cannot be estimated as such. One of the approaches to deal with the unstructured uncertainties, is to use a control that does not excite these lags as done in [9]. The approach used in this paper is based on the following rationale. The unmodeled lags affect the system in two ways, viz. 1) distorting the input signal due to an unmodeled actuator and/or 2) distorting the output signal due to the flexibility effects or the sensor dynamics. Therefore, if the unmodeled lags are fast, their effects can be mitigated by obtaining the states through an observer. If the observer used is of the Luenberger type, it will be sensitive to structured uncertainties and external disturbances. The ESO used in this paper performs better than the Luenberger observer because it can suppress the effects of unmodeled lags while retaining insensitivity to structured uncertainties and disturbances. It is worth noting that in [25], Bondarev et al. have shown the effect of Luenberger type observer on systems with unmodeled dynamics and in [26] Zak et al. have extended the argument for observers that can tackle structured uncertainties explicitly using a sliding mode observer.

D. Augmentation of LQR Controller

In view of the results presented in the last section, it becomes obvious that in the presence of unmodeled dynamics, the LQR controller of Eq. (6) can be made useful by using it with the estimated states. However, one needs to address the problem of degradation in the performance of the controller in the presence of an external disturbance as seen in Fig. 5. One approach to address the latter issue is to estimate the effect of the external disturbance and use the estimate to augment the controller. To this end, the LQR controller of Eq. (6) is augmented using estimated states and the estimated disturbance as

$$u = -K\hat{x}_p - \frac{1}{b_o}\hat{d} \tag{8}$$

The controller of Eq. (8) is robust as it caters to the effects of disturbances and uncertainties and unmodeled dynamics but it cannot be implemented unless the estimates of states as well as the

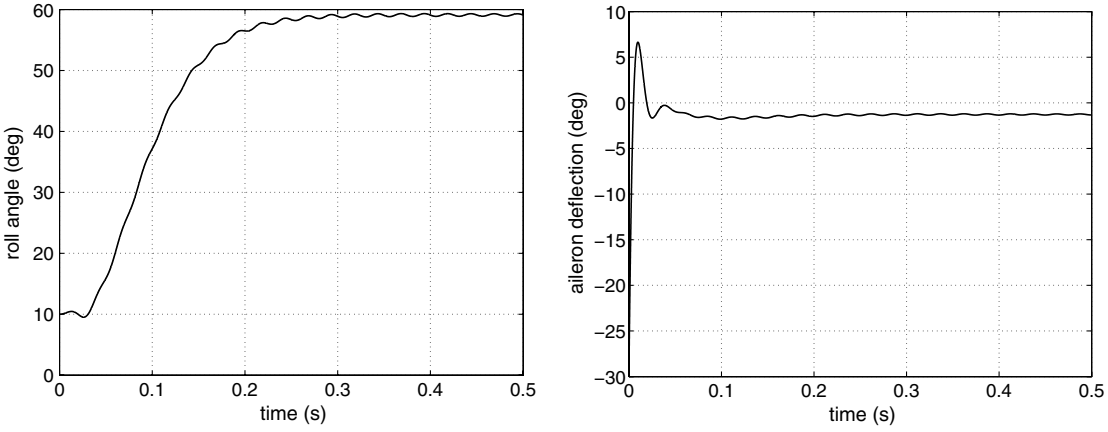

a) b)

Fig. 5 Performance of LQR + LO controller with flexibility dynamics and external disturbance.

disturbance is available. In the next section we show how these estimates can be obtained using the ESO.

III. ESO-Based Roll Autopilot Design

As stated earlier, the ESO is an observer which can estimate the effects of uncertainties and disturbances along with the states of the system enabling disturbance rejection or compensation. Unlike traditional (linear or nonlinear) observers, the ESO estimates the uncertainties and the disturbances acting on the system as an extended state of the original system. Because the observer estimates the uncertainties and the disturbances as an extra state, it is designated as ESO. Its merit is that it is relatively independent of a mathematical model of the plant, performs better and is simpler to implement. The robustness is inherent in its structure as will be obvious in the next section. In [22], a comparative study of the performances and characteristics of three advanced state observers, namely high gain observer, ESO, and sliding mode observer, is presented and it is shown that over all the ESO is superior in dealing with the uncertainties, disturbances, and the sensor noise.

Several diverse applications of ESO-based control strategies have appeared in the literature. Application of ESO to robotic hand–eye coordination [28], control of a flexible joint system [29], precision motion control [30], aircraft attitude control [31], and torsional vibration control of the main drive system of a rolling mill [32], are some examples to mention. In this section a brief review of this approach and its application to estimation of states and the uncertainty in the present problem are presented.

A. Concept of ESO

Consider an nth-order, single-input, single-output nonlinear dynamical system described by

$$\overset{(n)}{y} = a(y, \dot{y}, \cdots, \overset{(n-1)}{y}, w) + bu \tag{9}$$

where $a(.)$ represents the dynamics of the plant and the disturbance, $w(t)$ is an unknown disturbance, u is the control signal, and y is the measured output. Let $a(.) = a_o(.) + \Delta a$ and $b = b'_o + \Delta b$ where $a_o(.)$ and b'_o are the best available estimates of a and b, respectively, and Δa and Δb are their associated uncertainties. Defining the uncertainty to be determined as $d \triangleq \Delta a + \Delta b u + w$ and designating it as an extended state, x_{n+1}, the dynamics given by Eq. (9) can be rewritten in the state-space form as

$$\begin{aligned}
\dot{x}_1 &= x_2 \\
\dot{x}_2 &= x_3 \\
&\vdots \\
\dot{x}_n &= x_{n+1} + a_o + b'_o u \\
\dot{x}_{n+1} &= h \\
y &= x_1
\end{aligned} \tag{10}$$

where h is the rate of change of the uncertainty, i.e., $h = \dot{d}$ and is assumed to be an unknown but a bounded function. By making d a state, it is now possible to estimate it using a state estimator. To this end, consider a nonlinear observer of the form

$$\begin{aligned}
\dot{\hat{x}}_1 &= \hat{x}_2 + \beta_1 g_1(e_{o_1}) \\
\dot{\hat{x}}_2 &= \hat{x}_3 + \beta_2 g_2(e_{o_1}) \\
&\vdots \\
\dot{\hat{x}}_n &= \hat{x}_{n+1} + \beta_n g_n(e_{o_1}) + a_o + b'_o u \\
\dot{\hat{x}}_{n+1} &= \beta_{n+1} g_{n+1}(e_{o_1})
\end{aligned} \tag{11}$$

where $e_{o_1} = y - \hat{x}_1 = x_1 - \hat{x}_1$ and $\hat{x}_{n+1}$ is an estimate of the uncertainty d. The quantities β_i are the observer gains while $g_i(.)$ is a set of suitably constructed nonlinear gain functions satisfying $e_{o_1} g_i(e_{o_1}) > 0$, $\forall\ e_{o_1} \neq 0$ and $g_i(0) = 0$. If one chooses the nonlinear functions $g_i(.)$ and their related parameters properly, the estimated state variables $\hat{x}_i$ are expected to converge to the respective states of the system x_i, i.e., $\hat{x}_i \to x_i$; $i = 1, 2, \ldots, n+1$.

The choice of the nonlinear function is an important aspect in the ESO design. The general expression for these functions, selected heuristically based on experimental results [22] is

$$\begin{aligned}
g_i(e_{o_1}, \mu_i, \epsilon) &= \begin{cases} |e_{o_1}|^{\mu_i} \operatorname{sign}(e_{o_1}), & |e_{o_1}| > \epsilon \\ \frac{e_{o_1}}{\epsilon^{1-\mu_i}}, & |e_{o_1}| \leq \epsilon \end{cases} \\
i &= 1, 2, \ldots, n+1
\end{aligned} \tag{12}$$

where $\epsilon > 0$. An important property of these functions is that for $0 < \mu_i < 1$, $g_i(.)$ yields a relatively high gain when the error is small and a small gain when the error is large. The constant ϵ is a small number used to limit the gain in the neighborhood of the origin and defines the range of the error corresponding to the high gain.

B. Linear ESO

The ESO given by Eq. (11) with the gains given in Eq. (12), is called the nonlinear ESO or NESO as it employs nonlinear gain functions. On the other hand if one chooses $g_i(e_{o_1}) = e_{o_1}$, the ESO takes the form of the conventional Luenberger observer and is designated as the linear ESO (LESO). It can be noted that the LESO essentially represents a special case of the nonlinear ESO if one chooses the NESO parameters μ_is as unity. For linear dynamics, $a(.)$ in Eq. (9) is linear in its arguments, i.e., $a_o(.) = -a_{no}x_1 - a_{(n-1)o}x_2 \cdots a_{1o}x_n$. In view of this the extended order system Eq. (10), written in the state-space notation gives

$$\dot{x} = Ax + Bu + Eh \qquad y = Cx \tag{13}$$

where $x = [x_1 \quad x_2 \quad \cdots \quad x_n \quad x_{n+1}]^T$ is the state vector of the extended order system and

$$A = \begin{bmatrix} 0 & 1 & 0 & \cdots & 0 \\ 0 & 0 & 1 & \cdots & 0 \\ & & \ddots & & \\ -a_{no} & -a_{(n-1)o} & \cdots & -a_{1o} & 1 \\ 0 & 0 & \cdots & 0 & 0 \end{bmatrix}$$

$$B = \begin{bmatrix} 0 \\ 0 \\ \vdots \\ b'_o \\ 0 \end{bmatrix}; \qquad E = \begin{bmatrix} 0 \\ 0 \\ \vdots \\ 0 \\ 1 \end{bmatrix}$$

and $C = [1 \quad 0 \quad 0 \quad \cdots \quad 0]$. The LESO for the system of Eq. (13) is given by Eq. (11) with the gains $g(e_{o_1}) = e_{o_1}$. The state-space model of the LESO dynamics can be written as

$$\dot{\hat{x}} = A\hat{x} + Bu + LC(x - \hat{x}) \tag{14}$$

where

$$L = [\beta_1 \quad \beta_2 \quad \cdots \quad \beta_n \quad \beta_{n+1}]^T \tag{15}$$

is the observer gain vector.

It may be noted that the pair (A, C) is observable. Defining e_i as the ith position vector, i.e., a column vector given by $[0 \quad 0 \quad \ldots \quad 1 \quad \ldots \quad 0 \quad 0]^T$ where the element 1 appears in the ith row, the matrices C and A can be expressed as

$$C^T = e_1 \quad \text{and} \quad A^T = [e_2 \quad e_3 \quad \ldots \quad e_{n-1} \quad e_n \quad z_1 \quad z_2] \tag{16}$$

where z_1^T and z_2^T are, respectively, the nth and $(n+1)$th rows of A. The observability matrix V is

$$V = [C^T A^T C^T ... (A^T)^{n-1} C^T (A^T)^n C^T] \tag{17}$$

$$= [\, e_1 \quad e_2 \quad \ldots \quad e_n \quad z_1 \,] \tag{18}$$

It is easy to see that the V matrix has all diagonal elements equal to 1 and all elements below the diagonal equal to 0. Thus the matrix V is of full rank. This proves that the pair (A, C) is observable.

In the present work, LESO is employed instead of the NESO as linear ESO appears to be adequate. The LESO is easy to implement in hardware. as shown in [29]. However, the potential of NESO needs to be explored further and can be a subject of interesting research. It is with this purpose that the NESO is presented here.

C. LESO-Based Roll Controller

Now consider the roll dynamics of Eq. (4) and the augmented LQR controller given by Eq. (8). A linear ESO is designed to obtain the estimates of the state and the disturbance. The extended order dynamics of Eq. (4) is given by Eq. (13) with $n = 4$ and the corresponding ESO is given by Eq. (14) with $n = 4$ and $b_o = b'_o$. With the estimates, the controller of Eq. (8) takes the form

$$u = -K\hat{x}_p - \frac{1}{b_o}\hat{x}_5 \tag{19}$$

where $\hat{x}_5$ is an estimate of the effect of uncertainties and external disturbances d. The controller of Eq. (19) is designated as the ESO-based controller and is implementable. Noting that $x = [\, x_p \quad x_5 \,]^T$ and $\hat{x} = [\, \hat{x}_p \quad \hat{x}_5 \,]^T$, the controller of Eq. (19) can also be written as

$$u = -\bar{K}\,\hat{x} \tag{20}$$

where $\bar{K} \triangleq [\, K \quad \frac{1}{b_o} \,]^T$ is the effective state feedback gain vector.

In view of Eqs. (14) and (20), it can be easily verified that the ESO-based observer and the LQR based controller structure can be represented in state-space form as shown in Fig. 1e.

IV. Closed-Loop Stability

In this section, the closed-loop stability of the system of Eq. (4) is proved under the controller-observer combination, wherein the controller is given by Eq. (19) and the observer is given by Eq. (14) with $n = 4$. Now consider the roll dynamics of Eq. (4)

$$\dot{x}_p = A_p x_p + B_p u + B_d d \tag{21}$$

and the controller given by Eq. (19)

$$u = -K\hat{x}_p - \frac{1}{b_o}\hat{x}_5 \tag{22}$$

Using Eqs. (21) and (22), one can work out the following error dynamics:

$$\dot{x}_p = (A_p - B_p K)x_p + [\, B_p K \quad B_d \,]e_o \tag{23}$$

where e_o is the observer estimation error vector, i.e., $e_o = x - \hat{x}$.

Next the observer error dynamics is obtained by subtracting Eq. (14) from Eq. (13) with $n = 4$ as

$$\dot{e}_o = (A - LC)e_o + Eh \tag{24}$$

Combining Eqs. (23) and (24) gives

$$\begin{bmatrix} \dot{x}_p \\ \dot{e}_o \end{bmatrix} = \begin{bmatrix} (A_p - B_p K) & [\, B_p K \quad B_d \,] \\ 0 & (A - LC) \end{bmatrix} \begin{bmatrix} x_p \\ e_o \end{bmatrix} + \begin{bmatrix} 0 \\ E \end{bmatrix} h \tag{25}$$

As the system matrix in Eq. (25) is in block-triangular form, it is straightforward to verify that the eigenvalues of the system matrix of the error dynamics are given by the eigenvalues of $(A_p - B_p K)$ and $(A - LC)$. Because the pair (A_p, B_p) is controllable and the pair (A, C) is observable, stability of the error dynamics of Eq. (25) can always be ensured by placing the controller and observer poles appropriately. Further, because Eq. (25) is stable, it is obvious that under the assumption of boundedness of h, the bounded input-bounded output stability for the linear system of Eq. (25) is assured. A special case arises when $h = 0$, i.e., when the rate of change of the uncertainty d, is zero. In this case, the error dynamics of Eq. (25) is asymptotically stable. A similar result can be expected if the rate of change of the uncertainty is reasonably small.

It is to offer some comments on the performance of ESO when the rate of change of uncertainty is not negligible. The ESO error dynamics of Eq. (24) is asymptotically stable under the assumption that the rate of change of uncertainty h is negligible. The assumption does not hold good for systems affected by fast varying disturbances/uncertainties or for systems having state dependent uncertainties and are excited by fast varying reference signals. In these situations the performance of the ESO presented in Sec. III.B may not offer satisfactory results. However, the issue of the fast varying uncertainties too can be dealt within the framework of the ESO by employing a higher-order ESO [33]. For example, if the rate of change of uncertainty is not negligible, but its second rate is, then a second-order ESO can be employed. It can be proved that the estimation error dynamics for the second-order ESO will be asymptotically stable if $\ddot{d}$ is negligible. As a matter of fact, one can design an rth-order ESO if the rth rate of change of uncertainty is negligible.

V. Simulations and Results

Simulations are carried out to verify the performance of the ESO as an estimator of states and disturbances and that of the ESO-based controller as a regulator in a realistic scenario. To this end, the LQR controller gain K required in Eq. (19), is obtained by taking the weightings Q and R given in Eq. (7) with the values for $\phi_{\max}$, $\dot{\phi}_{\max}$, and $\delta_{c(\max)}$ taken from Table 1. The ESO gains, β_is are obtained by placing the observer poles at -45. Assuming that there exists an initial roll angle of 10°, the initial conditions for the plant are taken as $x_p(0) = [\, 10^\circ \quad 0 \quad 0 \quad 0 \quad 0 \,]^T$. Because the roll angle is a measured quantity, it is known and thus the initial conditions for the ESO are taken as $\hat{x}(0) = [\, 10^\circ \quad 0 \quad 0 \quad 0 \quad 0 \,]^T$. It is assumed that the missile is acted upon by a disturbance moment L_d, resulting in a disturbance roll acceleration of $d_{\text{ext}} = 200$ rad/s^2. First, to demonstrate the efficacy of the ESO in estimation of the states and the disturbance, only the external disturbance is considered as shown in the system block diagram of Fig. 1d and the results for this case are given in Fig. 6. In Figs. 6a–6d, the estimated states are plotted along with the actual ones and it can be seen that the ESO estimates the states satisfactorily. Also from Fig. 6a it can be noted that the controller has regulated the roll angle to zero as desired.

Next, we verify the performance of the ESO in estimation of the external disturbance. As shown in Fig. 1d, while the considered external disturbance d_{ext} acts in the roll moment channel, the disturbance d of Eq. (5) appears in input channel. Thus for a valid comparison, it is necessary to compute an equivalent disturbance that acts in the input channel from the considered disturbance, d_{ext}. To this end, one can show that the equivalent disturbance acting in the input channel, d_{eq} is related to d_{ext} by

$$d_{\text{eq}} = \omega_A^2 d_{\text{ext}} + 2\zeta_A \omega_A \dot{d}_{\text{ext}} + \ddot{d}_{\text{ext}} \tag{26}$$

As d_{ext} is constant, d_{eq} is also constant and is given by $\omega_A^2 d_{\text{ext}}$. One can calculate d_{eq} by using $\omega_A = 100$ and $d_{\text{ext}} = 200$ rad/s^2 as $d_{\text{eq}} = 2 \times 10^6$ rad/s^4 $= 11.46 \times 10^7$ deg/s^4. Now, observing the time histories of the actual and the estimated disturbance given in Fig. 6e, it is clearly seen that the ESO has estimated the equivalent disturbance accurately. From the roll dynamics shown in Fig. 1d, the steady-state aileron angle that would be required to counter the external disturbance of d_{ext} can be obtained as

$$\delta \approx -\frac{d_{\text{ext}}}{K_\delta} \tag{27}$$

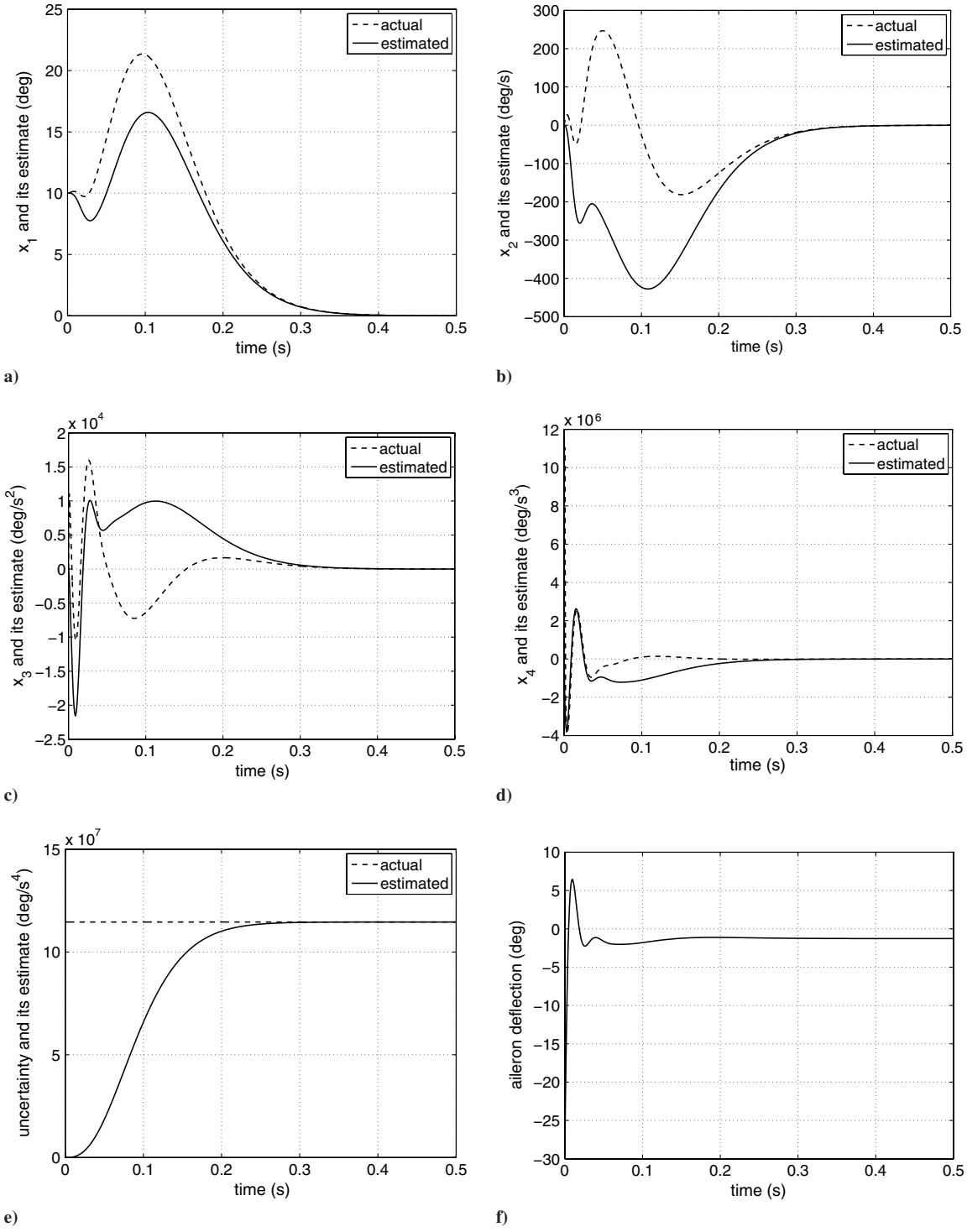

Fig. 6 Performance of ESO-based controller with external disturbance: State and uncertainty estimation and regulation.

which, with $d_{\text{ext}} = 200$ and $K_\delta = 9000$, comes out to be -0.0222 rad or $-1.27°$ approximately. The time history of the commanded aileron angle is given in Fig. 6f from where it can be noted that the steady-state aileron angle is $-1.27°$ as expected.

Now simulations are carried out to demonstrate the effectiveness of the ESO-based controller in a more realistic situation. To this end, apart from the unmodeled dynamics (flexibility and rate gyro dynamics) and the external disturbance, parametric uncertainty of $\pm 20\%$ in fin effectiveness K_δ, is included as shown in Fig. 1e. Further, it is assumed that the rate gyro measurement is corrupted by a zero mean white noise of standard deviation of 0.0167 deg/s [34]. The simulations results are presented in Fig. 7 from where it becomes obvious that the ESO-based controller has offered satisfactory performance notwithstanding the considered uncertainties and disturbances.

Next, to show that the ESO-based controller can cater for much larger parametric uncertainty, simulations are carried out by considering the measurement noise along with the flexibility and the rate gyro dynamics, the external disturbance and a parametric uncertainty of $\pm 40\%$ in K_δ and the results are shown in Fig. 8. From the figures, one can note that the ESO has offered satisfactory performance in roll regulation. With this capability, it is expected that the number of operating points required for gain scheduling the ESO-based controller will be significantly less than many other approaches. In all the above simulations, it may also be noted that the commanded aileron angle does not exceed 30° in magnitude, as desired.

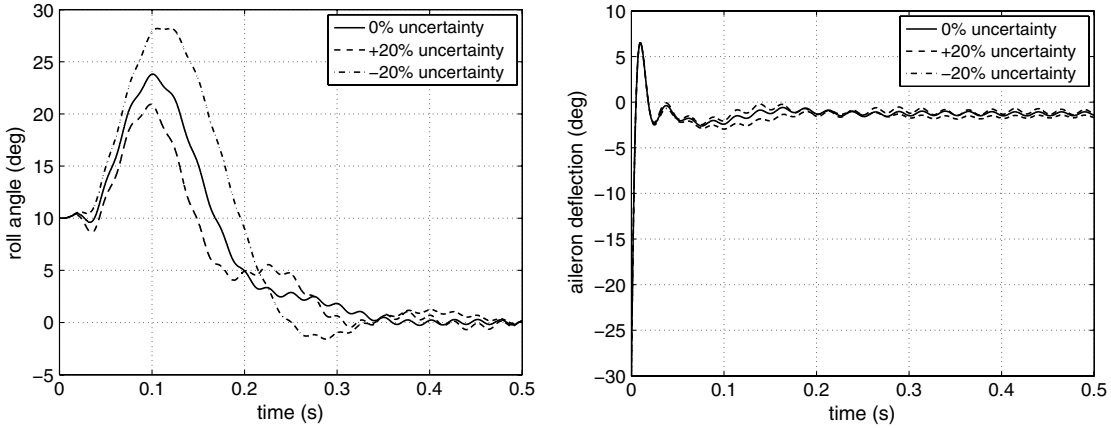

a) b)

Fig. 7 Performance of ESO-based controller with flexibility and rate gyro dynamics, external disturbance, sensor noise and ±20% uncertainty.

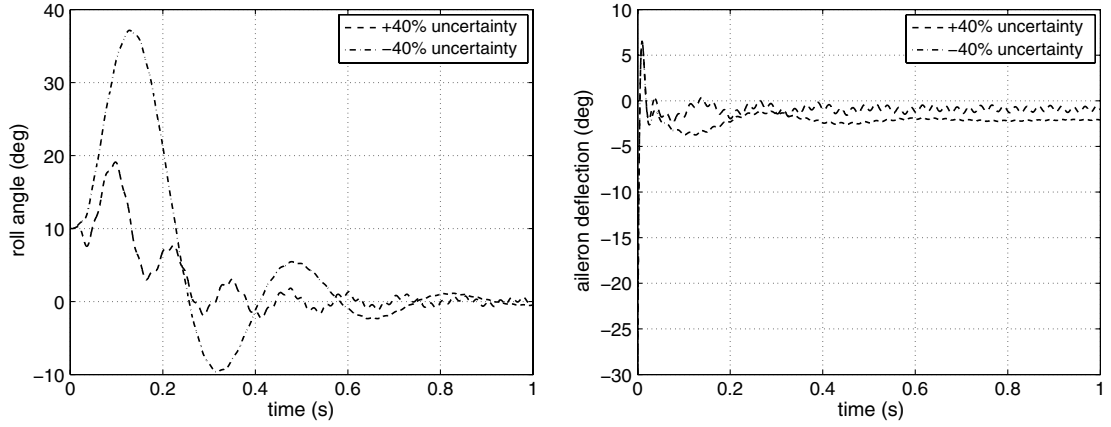

a) b)

Fig. 8 Performance of ESO-based controller with flexibility and rate gyro dynamics, external disturbance, sensor noise and ±40% uncertainty.

VI. Comparison with Existing Designs

The last objective is to compare the performance of the proposed ESO-based roll autopilot design with the ones existing in the literature. To this end, a comparison of the proposed design with the designs given in [8,9] is carried out. A brief outline of the designs is given below for the sake of convenience and the readers may consult the references for more details.

Design-1:

In [8], a design of roll autopilot based on the classical approach is presented wherein the autopilot is designed to achieve maximum crossover frequency for given bandwidths of the servo, the rate gyro and the first torsional mode. The crossover frequency is chosen high enough to ensure a wide autopilot bandwidth but low enough to prevent stability problems. To counteract the effect of the torsional mode on limiting the crossover frequency, a notch filter is designed. The resulting controller with the roll rate as the output is a proportional integral (PI) controller of the form

$$G_c(s) = F_1 + \frac{F_2}{s} \tag{28}$$

For the design goal of achieving a phase margin of 30 deg, and for the data given in Table 1, the gains of the controller are selected and are as given in Table 2. The design is designated as Design-1.

Design-2:

Reference [8] also presents a combined optimal/classical design for a roll autopilot wherein a simplified model is used for the optimal design with the classical design techniques supplying some additional constraints. For the optimal design, only a second-order rigid body roll dynamics is considered for the design of an LQR controller. The classical design involves the design of a notch filter and specifying constraints such as crossover frequency so that the design remains stable in the presence of high frequency dynamics. The constraints are used to bound the parameters of the performance index, resulting in a combined optimal/classical design. The resulting controller is also a PI controller as given by Eq. (28). For

Table 2 Simulation parameters

Design	Gains		ω_{gc} (rad/s)	Gain margin, dB	Phase margin, deg
Design-1	$F_1 = 0.0033$	$F_2 = 0.0367$	32.5	5.30	32.6
Design-2	$F_1 = 0.0037$	$F_2 = 0.0530$	36.9	3.92	23.5
Design-3	$F_1 = 0.0500$	$F_2 = 0.0035$	35.5	5.76	33.1
Design-4	-	-	33.8	3.95	18.0
Design-5	$F_1 = 0.0033$ $F_3 = 0.1500$	$F_2 = 0.0367$	31.3	5.38	32.9

achieving gain crossover of 33 rad/s, and for the data given in Table 1, the gains of the controller are as given in Table 2. The design is referred to as Design-2.

Design-3:

In [9], an LQR controller is designed by using the rigid body, second-order roll dynamics given by Eq. (1). The authors have shown that the gain crossover frequency can be controlled by adjusting some parameters, especially the weighting on the control input, in the LQR performance index. To this end, the weighting on the control input in the performance measure is adjusted by tuning $\delta_{c\max}$ to achieve the desired gain crossover frequency. The resulting controller is a two state controller, and thus has a similar form as given by Eq. (28). For the data given in Table 1, and with $\delta_{c\max} = 0.5$ deg, the gains of the controller are as given in Table 2. This design is referred to as Design-3.

Design-4:

The proposed ESO-based design is designated as Design-4 for the purpose of comparison. Throughout this work, the LQR controller gains are computed using Eq. (7) and the data given in Table 1. The resulting closed-loop poles are at -30, -202, and $-104.24 \pm$ j182.91. The ESO observer gains are chosen by following the guideline that the observer bandwidth be higher than the controller bandwidth. Also the observer bandwidth should be sufficiently small so as to avoid stability problems when unmodeled dynamics is considered. To this end, noting that the dominant closed-loop pole of the system is at -30 and with an objective of achieving a phase margin of about 20 deg, the poles of the observer dynamics are selected at -45 and the same has been used throughout this work.

Design-5:

Design-1, described earlier in this section, represents a roll rate control loop employing a PI controller which can also be interpreted as a roll position control loop with a PD controller. In this design, the addition of an integral action is expected to reduce the roll angle error induced by a disturbance moment to zero. Therefore, an integral controller with a gain of F_3 is introduced along with the PD controller used in the design of Design-1. The gains F_1 and F_2 are kept the same as Design-1, the integrator gain F_3 is tuned to 0.15 so as to achieve a phase margin close to that in Design 1.

To compare the performance, simulations are carried out by considering the data given in Table 1 for all the designs. The data for the notch filter, taken from [8] and used in the simulations of Design-1 and 2, is given in Table 1. For simulations of Designs-1–3, the block diagram is essentially the same as shown in Fig. 1e except that the PI controller and the notch filter precede the actuator block and replace the observer-controller structure appearing in the feedback path. Also as the controller is PI, the rate gyro output is fed back instead of the roll angle shown in Fig. 1e. For simulations of Design-4, the same block diagram given in Fig. 1e is employed. The block diagram used in simulation for the Design-5 is essentially the same as that of the Design-1 with an additional integration loop as explained earlier. In simulations, the flexibility and the rate gyro dynamics, the parametric uncertainty of $\pm 20\%$ in fin effectiveness K_δ and the external disturbance are considered. Also notch filters are included in simulations of Designs-1 and 2 and the results are presented in Fig. 9. From the figures, it becomes obvious that while the Designs-1–3 have resulted in a large steady-state error in the roll angle, the ESO-based controller has offered satisfactory roll regulation. It can also be observed, that while the Design-5, eliminates the roll angle error in response to a constant disturbance, the transient errors and settling time are significantly larger in comparison to the ESO-based design.

It is known that the effect of disturbance on error may be reduced if the LQR gains are increased. However, the increase in the gains may result in stability problems when unmodeled dynamics are considered. Thus, in this approach the requirement of robustness to external disturbances inherently conflicts with the requirement of robustness to fast unmodeled dynamics.

Lastly, frequency response analysis is carried out and the results are tabulated in Table 2. From the table, it can be noticed that the phase margin of the proposed design is about 18 deg, which is less than the other designs. However, the phase margin may be considered satisfactory in the present application as all low-frequency lags likely to occur in such designs have been taken into account.

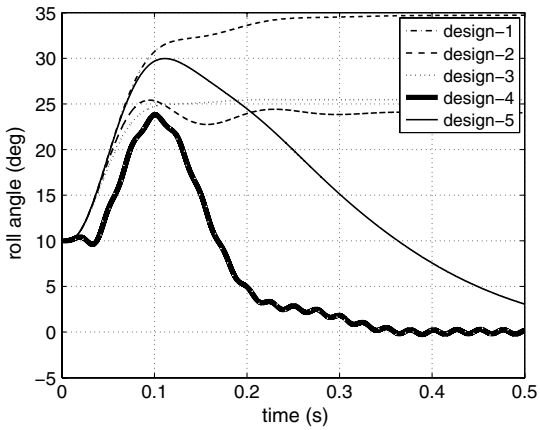

a)

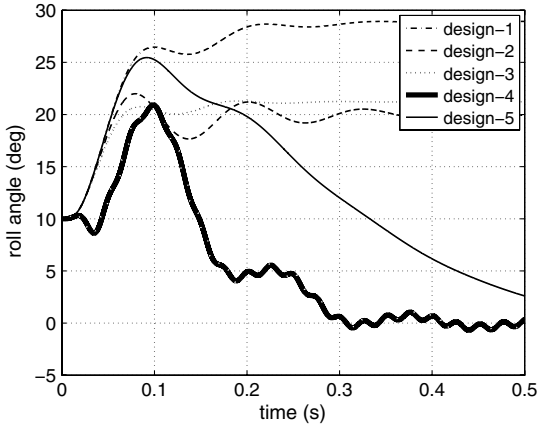

b)

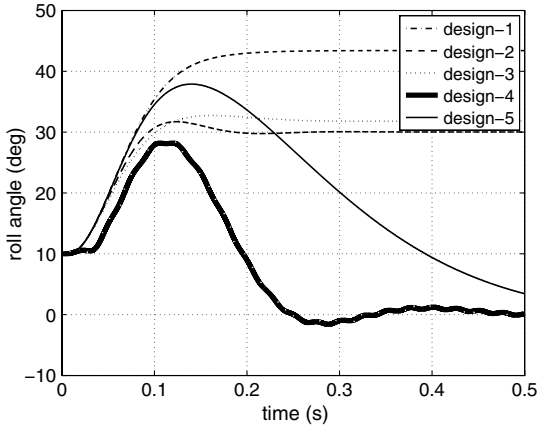

c)

Fig. 9 Performance comparison with existing designs with uncertainties (a) 0% (b) +20% (c) −20%.

VII. Conclusions

In this paper an ESO-based controller is proposed for the design of a robust roll autopilot. System states as well as the effect of uncertainties and the external disturbance acting on the system are estimated by the ESO in an integrated manner. An LQR controller designed for the nominal system, is augmented by the opposite of the estimate of the disturbance. Simulation results show that the proposed design is robust and offers satisfactory performance in the presence of large external disturbance, parametric uncertainties and unmodeled dynamics. Performance comparison of the proposed

design with the ones existing in the literature has shown that the former offers better disturbance rejection capabilities.

Acknowledgment

The authors would like to thank the anonymous reviewers for their comments and constructive suggestions, which have helped improve the quality of the paper.

References

[1] Garnell, P., *Guided Weapon Control Systems*, 2nd ed., Pergamon Press, Oxford, England, 1980.

[2] Lee, R. G., Garland-Collins, T. K., Johnson, D. E., Archer, E., Sparkes, C., Moss, G. M., and Mowat, A. W., *Guided Weapons, Vol. 1, of Land Warfare: Brassey's New Battlefield Weapons Systems and Technology Series*, 1st ed., Brassey's Defence Publishers, London, 1988.

[3] Horton, M. P., "Autopilots for Tactical Missiles: An Overview," *Proceedings of the Institution of Mechanical Engineers. Part I, Journal of Systems and Control Engineering*, Vol. 209, No. 29, 1995, pp. 127–139.
doi:10.1243/PIME_PROC_1995_209_373_02

[4] Zarchan, P., *Tactical and Strategic Missile Guidance*, 4th ed., Progress in Astronautics and Aeronautics, Vol. 199, AIAA, Reston, VA, 2002.

[5] Colgren, R., "Nonlinear H_∞ Control of a Missile's Roll Axis," *Proceedings of the American Control Conference*, IEEE Publications, Piscataway, NJ, June 1984, pp. 2109–2113.

[6] Buschek, H., "Full Envelope Missile Autopilot Design Using Gain Scheduled Robust Control," *Journal of Guidance, Control, and Dynamics*, Vol. 22, No. 1, Jan–Feb 1999, pp. 115–122.
doi:10.2514/2.4357

[7] Buschek, H., "Design and Flight Test of a Robust Autopilot for the IRIS-T Air-to-Air Missile," *Control Engineering Practice*, Vol. 11, No. 5, 2003, pp. 551–558.
doi:10.1016/S0967-0661(02)00063-1

[8] Nesline, F. W., Wells, B. H., and Zarchan, P., "Combined Optimal/Classical Approach to Robust Missile Autopilot Design," *Journal of Guidance, Control, and Dynamics*, Vol. 4, No. 3, 1981, pp. 316–322.
doi:10.2514/3.56084

[9] Nesline, F. W., and Zarchan, P., "Why Modern Controllers Can Go Unstable in Practice," *Journal of Guidance, Control, and Dynamics*, Vol. 7, No. 4, Jul–Aug 1984, pp. 495–500.
doi:10.2514/3.19884

[10] Ohta, H., and Kakinuma, M., "Use of Negative Weights in Linear quadratic Regulator Synthesis," *Journal of Guidance, Control, and Dynamics*, Vol. 14, No. 4, Jul–Aug 1991, pp. 791–796.
doi:10.2514/3.20714

[11] Williams, D. E., Friedland, B., and Madiwale, A. N., "Modern Control Theory for Design of Autopilots for Bank-to-Turn Missiles," *Journal of Guidance, Control, and Dynamics*, Vol. 10, No. 4, Jul–Aug 1987, pp. 378–386.
doi:10.2514/3.20228

[12] Roddy, D. J., Irwin, G. W., and Wilson, H., "Optimal Controllers for Bank-to-Turn CLOS Guidance," *IEEE Proceedings-Part D, Control Theory and Applications*, Vol. 131, No. 4, July 1984, pp. 109–116.
doi:10.1049/ip-d.1984.0020

[13] Jianbo, H., Hongye, S., and Jian, C., "Variable Structure Control for a Class of Fuzzy Dynamics and its Application to the Design of Autopilot for Missile," *Proceedings of the 3rd World Congress on Intelligent Control and Automation*, IEEE Publications, Piscataway, NJ, 2000, pp. 1615–1619.

[14] Tahk, M.-J., Briggs, M. M., and Menon, P. K. A., "Application of Plant Inversion via State Feedback to Missile Autopilot Design," *Proceedings of the 27th Conference on Decision and Control*, IEEE Publications, Piscataway, NJ, Dec. 1988, pp. 730–735.

[15] Calise, A. J., Sharma, M., and Corban, J. E., "Adaptive Autopilot Design for Guided Munitions," *Journal of Guidance, Control, and Dynamics*, Vol. 23, No. 5, Sept.–Oct. 2000, pp. 837–843.
doi:10.2514/2.4612

[16] Youcef–Toumi, K., and Ito, O., "A Time Delay Controller for Systems with Unknown Dynamics," *Transactions of the ASME, Journal of Dynamic Systems, Measurement, and Control*, Vol. 112, No. 1, 1990, pp. 133–142.
doi:10.1115/1.2894130

[17] Talole, S. E., Ghosh, A., and Phadke, S. B., "Proportional Navigation Guidance using Predictive and Time Delay Control," *Control Engineering Practice*, Vol. 14, No. 12, Dec. 2006, pp. 1445–1453.
doi:10.1016/j.conengprac.2005.11.003

[18] Talole, S. E., and Phadke, S. B., "Robust Input Output Linearisation using Uncertainty and Disturbance Estimation," *International Journal of Control*, Vol. 82, No. 10, Oct. 2009, pp. 1794–1803.
doi:10.1080/00207170902756552

[19] Talole, S. E., and Phadke, S. B., "Model Following Sliding Mode Control Based on Uncertainty and Disturbance Estimator," *Transactions of the ASME: Journal of Dynamic Systems, Measurement, and Control*, Vol. 130, No. 3, May 2008, pp. 1–5.
doi:10.1115/1.2909604

[20] Hall, C. E., and Shtessel, Y. B., "Sliding Mode Disturbance Observer-Based Control for a Reusable Launch Vehicle," *Journal of Guidance, Control, and Dynamics*, Vol. 29, No. 6, Nov.–Dec. 2006, pp. 1315–1328.
doi:10.2514/1.20151

[21] Han, J., "From PID to Active Disturbance Rejection Control," *IEEE Transactions on Industrial Electronics*, Vol. 56, No. 3, March 2009, pp. 900–906.
doi:10.1109/TIE.2008.2011621

[22] Wang, W., and Gao, Z., "A Comparison Study of Advanced State Observer Design Techniques," *Proceedings of the American Control Conference*, IEEE Publications, Piscataway, NJ, June 2003, pp. 4754–4759.

[23] Gao, Z., "Scaling and Bandwidth-Parametrization based Controller Tuning," *Proceedings of the American Control Conference*, IEEE Publications, Piscataway, NJ, 2003, pp. 4989–4996.

[24] Yoo, D., Yau, S. S.-T., and Gao, Z., "Optimal Fast Tracking Observer Bandwidth of the Linear Extended State Observer," *International Journal of Control*, Vol. 80, No. 1, 2007, pp. 102–111.
doi:10.1080/00207170600936555

[25] Bondarev, A. G., Bondarev, S. A., Kostyleva, N. E., and Utkin, V. I., "Sliding Modes in Systems with Asymptotic State Observers," *Avtomatika i Telemekhanika*, Vol. 6, June 1985, pp. 5–11; also *Automation and Remote Control*, Vol. 46, No. 6, June 1985, pp. 679–684 (in English).

[26] Zak, S. H., Brehove, J. D., and Corless, M. J., "Control of Uncertain Systems with Unmodeled Actuator and Sensor Dynamics and Incomplete State Information," *IEEE Transactions on Systems, Man, and Cybernetics*, Vol. 19, No. 2, March 1989, pp. 241–257.
doi:10.1109/21.31030

[27] Ogata, K., *Modern Control Engineering*, Prentice Hall of India, New Delhi, India, 1995.

[28] Su, J., Qiu, W., Ma, H., and Woo, P.-Y., "Calibration-Free Robotic Eye-Hand Coordination Based on an Auto Disturbance Rejection Controller," *IEEE Transactions on Robotics and Automation*, Vol. 20, No. 5, Oct. 2004, pp. 899–907.

[29] Talole, S. E., Kolhe, J. P., and Phadke, S. B., "Extended-State-Observer-based Control of Flexible-Joint System with Experimental Validation," *IEEE Transactions on Industrial Electronics*, Vol. 57, No. 4, April 2010, pp. 1411–1419.
doi:10.1109/TIE.2009.2029528

[30] Su, Y. X., Zheng, C. H., and Duan, B. Y., "Automatic Disturbances Rejection Controller for Precise Motion Control of Permanent-Magnet Synchronous Motors," *IEEE Transactions on Industrial Electronics*, Vol. 52, No. 3, June 2005, pp. 814–823.
doi:10.1109/TIE.2005.847583

[31] Huang, Y., Xu, K., Han, J., and Lam, J., "Flight Control Design Using Extended State Observer and Non-Smooth Feedback," *Proceedings of the 40th IEEE Conference on Decision and Control*, IEEE Publications, Piscataway, NJ, December 2001, pp. 223–228.

[32] Zhang, R., and Tong, C., "Torsional Vibration Control of the Main Drive System of a Rolling Mill Based on an Extended State Observer and Linear Quadratic Control," *Journal of Vibration and Control*, Vol. 12, No. 3, 2006, pp. 313–327.
doi:10.1177/1077546306063224

[33] Miklosovic, R., Radke, A., and Gao, Z., "Discrete Implementation and Generalization of the Extended State Observer," *Proceedings of the American Control Conference*, IEEE Publications, Piscataway, NJ, June 2006, pp. 2209–2214.

[34] Gurfil, P., "Synthesis of Zero Miss Distance Missile Guidance via Solution of an Optimal Tuning Problem," *Control Engineering Practice*, Vol. 9, No. 10, Oct. 2001, pp. 1117–1130.
doi:10.1016/S0967-0661(01)00057-0